

THE ROLE OF FIBRE ORIENTATION ON THE ELECTROMAGNETIC PERFORMANCE OF WAVEGUIDES MANUFACTURED FROM CARBON FIBRE REINFORCED PLASTIC

A. Bojovschi^{1, *}, K. J. Nicholson², A. Galehdar¹, P. J. Callus², and K. Ghorbani¹

¹School of Electrical and Computer Engineering, RMIT University, Melbourne, VIC 3001, Australia

²Air Vehicles Division, Defence Science and Technology Organisation, 506 Lorimer Street, Fishermans Bend, VIC 3207, Australia

Abstract—Aircraft skins manufactured from carbon fibre reinforced plastic (CFRP) can simultaneously support structural load and act as antennas. This offers the potential for disproportionately large antenna elements and arrays, and thus enhanced aircraft capability. The efficient design of such structures requires that the link between CFRP microstructure and electromagnetic performance be established. This paper presents a method of predicting the electromagnetic attenuation of waveguides manufactured from CFRP. The method considers both the orthotropic, complex conductivity of CFRP, high in the fibre direction and low transverse to it, and the local electric fields in waveguides, which vary with location and frequency. The method was validated experimentally using waveguides manufactured from aerospace grade IM7/977-3 prepreg tape with $[0\ 90]_s$, $[90\ 0]_s$ and $[\pm 45]_s$ ply stacking sequences.

1. INTRODUCTION

The quantum leap in aircraft performance achieved during the 1930's due to the replacement of fabric and wood structures with metallic components may be replicated by the adoption of multifunctional aircraft structures [1]. One type of multifunctional structure, known as Slotted Waveguide Antenna Stiffened Structure (SWASS), consists of slotted waveguide antennas integrated into aircraft skins. The

Received 11 January 2012, Accepted 7 March 2012, Scheduled 21 March 2012

* Corresponding author: Alexe Bojovschi (alex.bojovschi@rmit.edu.au).

skin both supports structural loads and acts as an antenna array. In contrast, traditional aircraft antennas consist of relatively massive mountings fastened to the external surface. This increases weight, creates drag and, if not covered with protective fairings or radomes, exposes the antenna directly to the environment. The incorporation of antennas into the structure solves these problems. In addition these antennas can be located over a greater proportion of the aircraft surface than their traditional counterpart. The larger area allows for disproportionately large arrays and antenna element sizes. The changed beam and frequency characteristics have the potential to enhance aircraft capability profoundly.

Carbon fibre reinforced plastic (CFRP) is used extensively in modern aircraft as a structural material. They have, relative to aluminium, lower weight, superior corrosion resistance, reduced susceptibility to fatigue damage, greater thermal stability and higher radar absorption [2, 3]. However the electrical conductivity of CFRP is lower than that of aluminium and this reduces the attractiveness of CFRP for electromagnetic applications.

One of the challenges in realising SWASS is to obtain the same or similar performances from CFRP waveguides as from traditional metallic waveguides. Diverse methods have been used previously to reduce the high electrical losses in CFRP waveguides. These have invariably involved applying a highly conductive metallic layer to the inside of the waveguide [4, 5] by processes such as electro-deposition [6] or sputtering [7]. These studies have highlighted the need to improve the RF conductivity of CFRP waveguides however, to date, there has been no fundamental study of this reported in the literature.

The current vectors in the walls of rectangular waveguides operating in the fundamental TE_{10} mode are oriented parallel and perpendicular to the longitudinal axis of the waveguide. The relative amplitude of these currents varies with frequency. This offers potential to tailor the orientation of orthotropic materials such as CFRP to minimise losses by aligning the direction of highest conductivity with the major current vectors.

This paper presents a method of predicting the attenuation constant of CFRP waveguides. It incorporates both the orthotropic, complex permittivity of the laminate and the variable currents on the waveguide walls. The model was validated using measurements on waveguides manufactured from aerospace grade CFRP prepreg tape with three different ply stacking sequences. This model may be used during the SWASS design process to assess, and optimise, the RF performance of CFRP waveguides.

2. COMPUTATIONAL APPROACH

Optimising the RF performance of CFRP waveguides requires an understanding of the field distribution within the waveguide and current distribution on the waveguide walls as well as the dependence of these variables on the material microstructure. These interactions were investigated using a Finite Element Method (FEM) [8–11] simulation as implemented in Ansoft High Frequency Structure Simulator (HFSS) [12].

2.1. Geometry of the Simulated CFRP Waveguides

The simulation model is shown in Figure 1. It consisted of a waveguide with cross-sectional dimensions of a and b and length d . Waveguide port 1 was used to excite the waveguide with a TE₁₀ mode, which is the dominant mode over the X-band (8 to 12 GHz). Waveguide port 2 was added to the opposite end of the waveguide to avoid reflections and to facilitate field calculation. The power at the waveguide ports was a time-averaged power. The waveguide ports simulated semi-infinite waveguides with the same cross-section as the waveguide under study. The waveguide was enclosed in a 50 mm thick layer of air, which itself was enclosed by a 78 mm thick Perfectly Matched Layer (PML). This ensured that electromagnetic radiation escaping the waveguide was attenuated and did not propagate back into the system.

The waveguide walls were divided into layers in order to account for the anisotropy of the CFRP plies. For each layer the effective

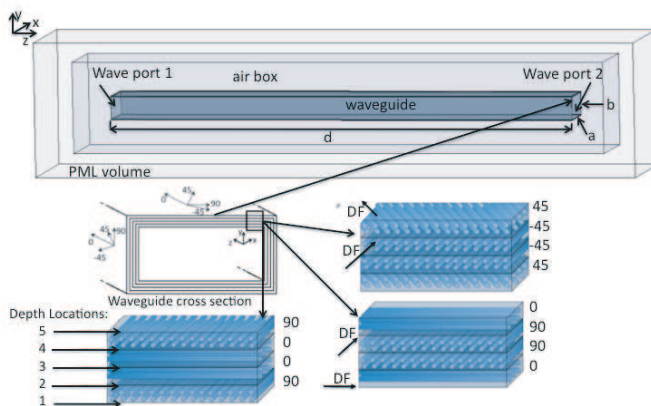


Figure 1. A schematic representation of the simulation geometry and the three ply stacking sequences, $[0\ 90]_s$, $[90\ 0]_s$ and $[\pm 45]_s$, with the direction of fibres (DF) presented.

conductivity and complex permittivity tensors were defined as specified in Section 2.2. The thickness of each layer was 125 μm , which corresponds to the thickness of a typical ply of aerospace grade CFRP prepreg tape. Three ply stacking sequences;

$$\begin{aligned} [0, 90]_s &= 0 \ 90 \ 90 \ 0, \\ [90, 0]_s &= 90 \ 0 \ 0 \ 90 \text{ and} \\ [\pm 45]_s &= +45 \ -45 \ -45 \ +45 \end{aligned}$$

were modelled. Schematic representations of these are presented in Figure 1. The 0° direction of fibres (DF) was parallel to the wave direction of propagation (waveguide z -direction). The 90° , 45° and -45° DF indicate that the fibres in the plies were perpendicular, or at 45° , to the symmetry planes of the waveguide as shown in Figure 1.

2.2. Computational Method and Simulation Parameters

CFRP plies are orthotropic in the x , y and z directions because they consist of unidirectional conductive carbon fibres surrounded by a matrix of dielectric polymer resin. The complex permittivity of IM7/977, an aerospace grade CFRP, [13] has been determined previously using surface resistance theory [14] and waveguide measurement methods [15]. The literature showed that unidirectional laminates are lossy with permittivities of $\varepsilon_{0^\circ} = \varepsilon_{90^\circ} = 30 - 7.4j$ and $\varepsilon_{45^\circ} = 32 - 9.2j$, the angles being between the carbon fibres and the incident wave. The study highlighted that CFRP plies are more conductive when the electric field is parallel to the direction of the fibres. In this work the complex permittivity is defined in the permittivity tensors (Equations (1), (2) and (3)) for 45° , 0° and 90° DF.

$$\varepsilon_{45a} = \begin{bmatrix} 0 & 0 & 0 \\ 0 & \varepsilon_{45y} & 0 \\ 0 & 0 & 0 \end{bmatrix} \quad \varepsilon_{45b} = \begin{bmatrix} \varepsilon_{45x} & 0 & 0 \\ 0 & 0 & 0 \\ 0 & 0 & \varepsilon_{45z} \end{bmatrix} \quad (1)$$

$$\varepsilon_{0a} = \varepsilon_{0b} = \begin{bmatrix} \varepsilon_{0x} & 0 & 0 \\ 0 & \varepsilon_{0y} & 0 \\ 0 & 0 & 0 \end{bmatrix} \quad (2)$$

$$\varepsilon_{90a} = \begin{bmatrix} 0 & 0 & 0 \\ 0 & \varepsilon_{90y} & 0 \\ 0 & 0 & \varepsilon_{90z} \end{bmatrix} \quad \varepsilon_{90b} = \begin{bmatrix} \varepsilon_{90x} & 0 & 0 \\ 0 & 0 & 0 \\ 0 & 0 & \varepsilon_{90z} \end{bmatrix} \quad (3)$$

where the complex permittivities are defined as:

$$\begin{aligned} \varepsilon_{0x} &= \varepsilon_{0y} = \varepsilon_{0z} = 30 - 7.4j \\ \varepsilon_{45x} &= \varepsilon_{45y} = \varepsilon_{45z} = 32 - 9.2j \\ \varepsilon_{90x} &= \varepsilon_{90y} = \varepsilon_{90z} = 30 - 7.4j \end{aligned}$$

The largest contributor to the conductivity of CFRP is fibre orientation. The diagonal and off-diagonal components of the effective conductivity tensor were defined for the CFRP layers in order to simulate the effect of this:

$$\sigma_{45a} = \begin{bmatrix} \sigma_{45x} & 0 & 0 \\ 0 & 0 & 0 \\ 0 & 0 & \sigma_{45z} \end{bmatrix} \quad \sigma_{45b} = \begin{bmatrix} \varepsilon_{45x} & 0 & 0 \\ 0 & 0 & 0 \\ 0 & \sigma_{45y} & 0 \end{bmatrix} \quad (4)$$

$$\sigma_{0a} = \sigma_{0b} = \begin{bmatrix} 0 & 0 & 0 \\ 0 & 0 & 0 \\ 0 & 0 & \sigma_{0z} \end{bmatrix} \quad (5)$$

$$\sigma_{90a} = \begin{bmatrix} \sigma_{90x} & 0 & 0 \\ 0 & 0 & 0 \\ 0 & 0 & 0 \end{bmatrix} \quad \sigma_{90b} = \begin{bmatrix} 0 & 0 & 0 \\ 0 & \sigma_{90y} & 0 \\ 0 & 0 & 0 \end{bmatrix} \quad (6)$$

where $\sigma_{45x} = \sigma_{45y} = \sigma_{45z} = \sigma_{0z} = \sigma_{90x} = \sigma_{90y} = 28,000 \text{ S/m}$ at 10 GHz. In (4) the conductivity is the same in the directions 45° , on the broad and short wall, 0° , on the broad wall and 90° on the short wall. This is due to the current flow distribution on the broad and short walls of the waveguide [16].

The conductivity of CFRP laminates was derived from the waveguide attenuation measurements (for the same ply stacking sequence) described in Section 3. Figure 2 shows the calculated values for $[0\ 90]_s$ in 0.5 GHz steps between 8.0 and 12.0 GHz. These data were approximated as the exponential decay $y = y_0 + A * \exp(-x/t)$ where $y_0 = 25429.336$, $A = 589538.054$ and $t = 1.825$. This equation was then used to calculate the diagonal elements in the tensors presented in (4), (5) and (6).

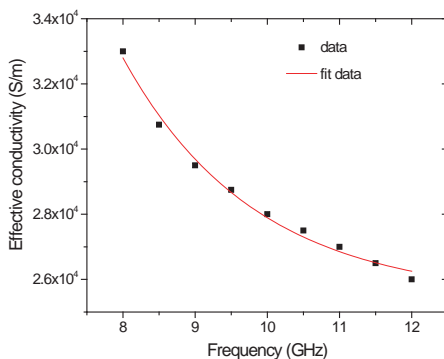


Figure 2. The effective conductivity of IM7/977-3 CFRP with a $[0\ 90]_s$ ply stacking sequence over the X-band.

3. EXPERIMENTAL APPROACH

The experimental work involved two steps. The first was to manufacture the CFRP waveguides and the second was to assess the electromagnetic performance of these waveguides by measuring their reflection and transmission coefficients. These two stages are detailed below.

Waveguide manufacture involved wrapping un-cured plies of Cytec IM7/977-3 prepreg tape [13] around a solid aluminium mandrel. The mandrel cross-section was identical to the interior cross-section of a WR90 waveguide (Figure 1) and the length was 300 mm. First prepreg ply had a length of 250 mm and a width of $2a + 2b$. This ensured that the ply could be wrapped around the mandrel once covering its entire surface, with no overlap at the seam. The second, third and fourth plies had the same length however the width was increased linearly to account for the thickening of the wrapped mandrel. The wrapped mandrel was vacuum bagged, to remove any air pockets, and then cured in an autoclave at 177°C and 586 kPa for 6 hours in accordance with the manufacturer's recommendation [17]. After curing and when the system reached room temperature the aluminium mandrel was removed. The ends of the waveguide were trimmed with a water cooled diamond saw to obtain a waveguide with a length of 200 mm. The wall thickness of the waveguide was approximately

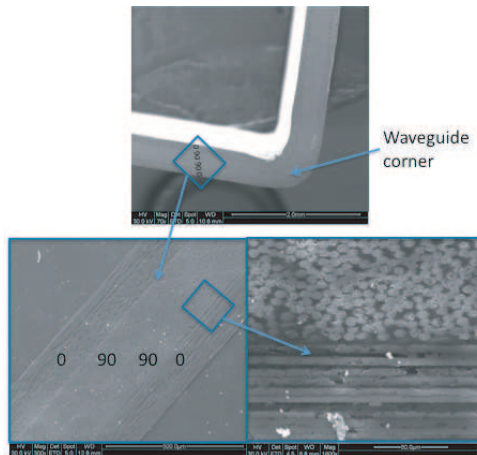


Figure 3. Cross section of a corner of $[0,90]_s$ waveguide which indicate the distribution of carbon fibres in the CFRP plies and the thickness of epoxy layer on the surface.

0.5 mm ($= 4 \times 125 \mu\text{m}$). Specimens were stored in ambient laboratory conditions, at approximately 40% relative humidity and 22°C, prior to testing.

The diameter of carbon fibre in the CFRP laminates averages $5 \mu\text{m}$ while the inter fibre epoxy has an average thickness of $1.2 \mu\text{m}$. Scanning Electron Microscopy imaging of the cross sections of the walls of the waveguides reveals the topological arrangement of the fibres in the CFRP layers (Figure 3). The thickness of epoxy skin on the laminate surface was approximately $5 \mu\text{m}$. This will vary according to surface roughness of the laminate. This thin layer is a dielectric with losses lower than carbon fibre therefore; small percentage of the energy is getting wasted. This indicates that the layer thickness is insignificant in terms of skin depth.

Twelve waveguides in total were produced using this method. These consisted of three batches of four waveguides each with ply stacking sequences of $[0\ 90]_s$, $[90\ 0]_s$ and $[\pm 45]_s$. Aluminium flanges were bonded to the ends of the waveguides using conductive epoxy. These were fastened to the ports of a Wiltron 360B vector network analyzer and the reflection, S_{11} , and transmission, S_{21} , coefficients measured. Equation (7) was used to calculate attenuation constant from measured S_{11} and S_{21} over the X-band (8 to 12 GHz):

$$\alpha = -10 \cdot \log (|S_{21}|^2 * (1 - |S_{11}|^2)) / L \quad (7)$$

where L was the length and equal to 1 m.

4. RESULTS AND DISCUSSIONS

The ability to transfer electromagnetic energy with minimal losses using waveguides revolutionised the telecommunications industry in the 1950's. These waveguides were traditionally fabricated from aluminium or copper. The losses in these waveguides occur in a thin layer at the surface called the skin-depth. Skin losses are the most important in waveguides and can be assessed by investigating the current densities.

The CFRP layers that form the walls of SWASS waveguides have an anisotropic conductivity. This is due to the orientation of the carbon fibres with reference to the symmetry axis of the waveguide and the lossy dielectric epoxy matrix that surrounds the carbon fibres. The leakage current through these layers affects directly the performance of the waveguides. The high conductivity of the CFRP layers along the fibres, called the in-plane conductivity, and small conductivity across the CFRP layers, called the out-of-plane conductivity, influences the performance of CFRP waveguides. Clearly the transmission efficiency

of CFRP waveguides is influenced by the properties of CFRP layers and the orientation of the carbon fibres.

The role of carbon fibre orientation on the attenuation constant is presented in Figures 4, 5 and 6. These figures show both experimental results and computational simulations based on the mathematical approximation of Figure 2. Good agreement was obtained for all three CFRP ply stacking sequences investigated. As mentioned in Section 3, the experimental results were for four waveguides of each configuration. Repeat measurements were conducted to account for

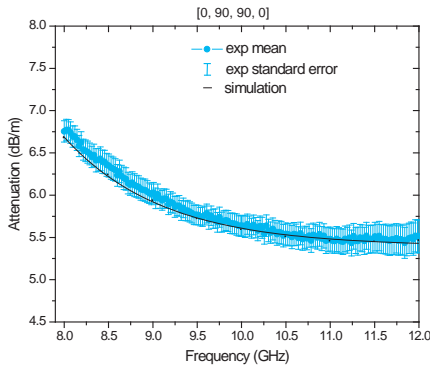


Figure 4. Attenuation within CFRP waveguides with a $[0\ 90]_s$ ply stacking sequence determined experimentally and computationally.

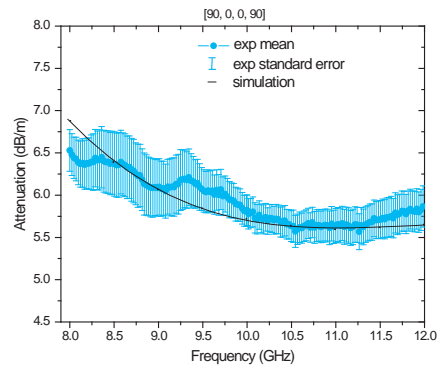


Figure 5. Attenuation within CFRP waveguides with a $[90\ 0]_s$ ply stacking sequence determined experimentally and computationally.

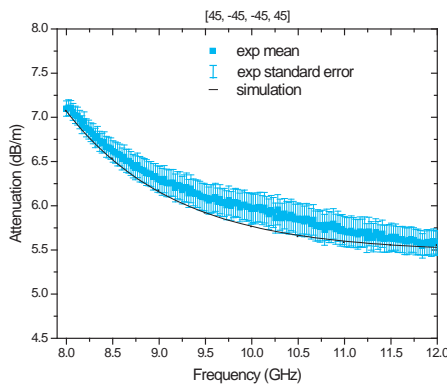


Figure 6. Attenuation within CFRP waveguides with a $[\pm 45]_s$ ply stacking sequence determined experimentally and computationally.

the error introduced in the fabrication process as well as the errors due to structural properties and morphology of carbon fibres in the CFRP. The average value (x_{av}) and the mean standard error ($SE_{\bar{x}}$) of the attenuation constant for the four similar waveguides were determined using:

$$x_{av} = \frac{1}{n} \sum_1^n x_i; \quad SE_{\bar{x}} = \frac{s}{\sqrt{n}} \tag{8}$$

$$s = \sqrt{\frac{1}{N-1} \sum_{i=1}^N (x_i - x_{av})^2} \tag{9}$$

where s is the sample standard deviation, n is the size of the sample, $\{x_1, x_2, \dots, x_N\}$ are the observed values of the sample items and x_{av} is the mean value of these observations.

The results plotted in Figures 4, 5 and 6 showed a similar trend, maximum attenuation at the lowest frequency, with a monotonic exponential decrease down to the minimum attenuation at maximum frequency. A selection of measured and predicted attenuation constants is shown in Table 1. Attenuation in the $[90\ 0]_s$ laminate was lowest in the range 8.0 to 8.5 GHz while for frequencies above this the $[0\ 90]_s$ laminate had lowest loss. The fluctuations in the attenuation constant for $[90,0]_s$ can be due to the contact between fibres from the two layers.

There was excellent agreement between the experimental measurements and predicted attenuation constants with predictions almost entirely within the one standard error of the experimental mean. In those cases where the predictions were outside this range, the difference may be explained by considering that the predictions were based on a least squares approximation of the conductivity. As shown in Figure 2, there was some difference between the experimentally measured conductivities and this least squares fit.

Table 1. Measured and predicted attenuation constants in waveguides manufactured from IM7/977-3 with the indicated ply stacking sequence and WR-90 internal cross-section.

Ply stacking sequence	Attenuation constant (dB/m) at indicated frequency					
	8 GHz		10 GHz		12 GHz	
	Meas.	Pred.	Meas.	Pred.	Meas.	Pred.
$[0\ 90]_s$	6.75	6.72	5.65	5.64	5.53	5.51
$[90\ 0]_s$	6.55	6.85	5.82	5.68	5.80	5.65
$[\pm 45]_s$	7.12	7.12	8.85	5.75	5.60	5.55

The attenuation of aluminium waveguides of the same size over this frequency band would be approximately 0.1 dB/m [18]. Attenuation in the CFRP waveguides was approximately two orders of magnitude greater than this. It is expected that such losses would make long lengths of CFRP waveguide unviable, however for shorter lengths it is entirely possible that losses will be tolerable. For example at 10 GHz the loss over 300 mm would be about 1.75 dB. This may be acceptable if the additional capability offered by SWASS exceeds the penalty of higher loss.

The exponential decay of the attenuation constants was due to power losses associated with the propagation of the TE_{10} mode down the rectangular waveguide. These losses are the sum of conductor and dielectric losses, both of which may be modelled by the perturbation method of the time-average loss power [16]. They are the time-average Joule's losses for the conductors in the walls and time-average power loss for the dielectric in the walls.

The ply stacking sequence influences directly the current density in the CFRP plies. Propagating electromagnetic waves induce electric currents in the waveguide walls [19]. These losses are greater if the conductivity is low in the direction of the electric field, as is the case when fibres are not parallel to the field. Some of the energy from refracted electromagnetic waves penetrates through the CFRP ply and part is lost as heat. The combination of these factors explains the different attenuation constants for the different ply stacking sequences.

The electromagnetic energy that flows through the walls of waveguides can be deduced from Maxwell equations. In 1884 J. H. Poynting showed that the flow of energy per unit area and per unit time equals $EH\sin\theta$ [20]. E and H are the magnitudes of the electric field intensities and θ is the angle between the vectors E and H . The flow of energy named also Poynting's vector through the wall of the waveguides with different fibre orientations is presented in Figure 7. The values of real Poynting vector on the inner and outer surface of the waveguide (Depth location 1 and 5) and at the interface between the layers (Figure 1) are quantified to provide a depth profile of the power level in the CFRP layer in the walls of the waveguides. The energy decays exponentially as it passes through the broad and short walls of the waveguide. These results are well correlated with the values of the attenuation constant. The power level on the outside of the walls is approximately three order of magnitude lower than that on the inside wall.

The peak values of current densities on the surface of the waveguide inner and outer walls were determined computationally and are shown in Figures 8 and 9 respectively. In general, as indicated in

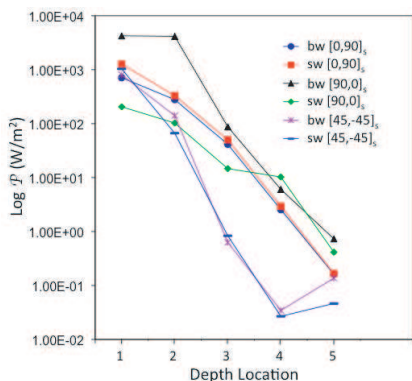


Figure 7. The maximum value of the real Poynting vector at different locations on the CFRP wall of the waveguide at 10 GHz. The abbreviations *bw* and *sw* refer to the waveguide broad- and short-wall respectively.

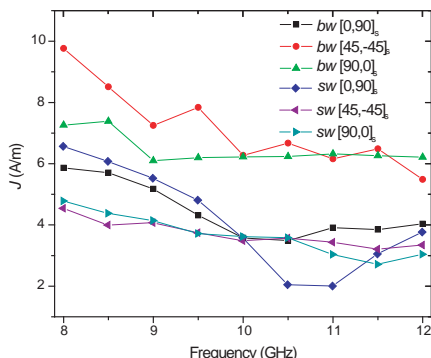


Figure 8. The maximum surface current density on the inner surface of the CFRP waveguides over the X-band. The abbreviations *bw* and *sw* refer to the waveguide broad- and short-wall respectively.

the literature [16], greater current was predicted to flow on the broad wall than the short wall. The opposite was predicted for the $[0\ 90]_s$ laminate below 10 GHz in the inner surface and 11.5 GHz on the outer surface.

The current density distribution in each the plies through-the-thickness in the broad and short walls were also predicted. For the shake of clarity these results will not be presented in this communication. Instead, the maximum value of the surface current density on the outer surface of the waveguides is shown in Figure 9. This is of relevance as it provides an explanation for the minimum values in the attenuation constant observed only for the $[90\ 0]_s$ waveguide structure at about 11 GHz. The surface current density between the broad and short wall for $[90\ 0]_s$ are larger compare to those at the centre of the of the X-band spectrum. These higher values of the current density indicate a higher loss through the walls of the waveguides. As is known the current density becomes zero as the skin depth is reached. Beyond the skin depth there should be no directional flow of electrons, instead their motion is govern by thermal effects. However for lossy materials, as is the case with CFRP, there is an electron flow beyond the expected skin depth. This causes the finite surface current densities presented in Figure 7. These currents are 0.01 to 0.05 A/m for $[\pm 45]_s$, 0.04 to 0.09 A/m for $[0\ 90]_s$ and 0.07 to 0.18 A/m for $[90\ 0]_s$. It should be noted that the lines that connect

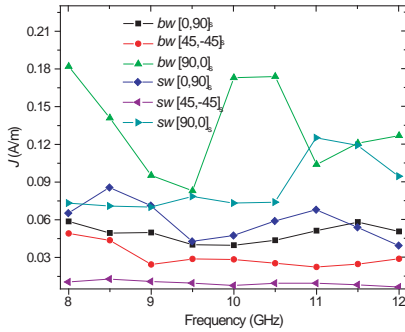


Figure 9. The maximum values of the surface current density on the outer surface of the CFRP waveguides over the X-band. The abbreviations *bw* and *sw* refer to the waveguide broad- and short-wall respectively.

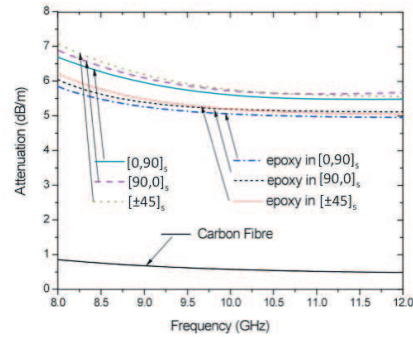


Figure 10. The attenuation constant in CFRP ($[0, 90]_s$, $[90, 0]_s$ and $[\pm 45]_s$) and carbon fibre waveguide (Carbon Fiber) and the attenuation constant due to losses in the epoxy resin (epoxy in $[0, 90]_s$, $[90, 0]_s$ and $[\pm 45]_s$) of the CFRP waveguides.

data points in Figures 7, 8 and 9 were added for shake of clarity and should not be assumed to reflect the true current densities.

The major losses in the CFRP are due to epoxy resin matrix. Determining the losses in a waveguide of only carbon fibre and subtracting the values from those in CFRP these losses can be estimated. The values of attenuation constant in a carbon fibre ($\sigma = 66666 \text{ S/m}$) [13] waveguide, of the same dimensions as the CFRP waveguide, are about 0.86 dB/m at 8 GHz and decrease exponentially to about 0.40 dB/m at 12 GHz (Figure 10). These lead to attenuation constants due to epoxy matrix smaller than those in CFRP by about 0.86 dB/m at 8 GHz , 0.58 dB/m at 10 GHz and 0.40 dB/m at 12 GHz as shown in Figure 10. The use of conductive intercalated compounds in the epoxy matrix that can reduce the losses while maintaining structural performance of CFRP it would be beneficial.

5. CONCLUSION

Tubes, having the same inner cross-section as WR-90 rectangular waveguides, were manufactured from aerospace grade IM7/977-3 carbon fibre reinforced plastic (CFRP) laminates with ply stacking sequences of $[0 \ 90]_s$, $[90 \ 0]_s$ and $[\pm 45]_s$. The electromagnetic attenuation of these waveguides was measured experimentally across the X-band and found to range from 5.5 to 7.2 dB/m . The lowest losses

from 8.0 to 8.5 GHz occurred in $[90\ 0]_s$ laminates and 8.5 to 12.0 GHz in $[0\ 90]_s$ laminates. These results were predicted well using an analytical modelling approach that considered both the (i) orthotropic conductivity tensor of CFRP that arises because conductivity is relatively high in the direction of the fibres and low transverse to this, and (ii) electric fields at the waveguide walls. Attenuation decreases when the fibres on the inner wall of the waveguide are oriented parallel to the local electrical field. The analytical model presented in this work can be used to optimise the electromagnetic design of waveguides manufactured from CFRP or any other anisotropic material where the effective conductivity and complex permittivity in three orthogonal coordinates are known.

ACKNOWLEDGMENT

The authors thank Professor Chun Wang and Dr Wayne Rowe for constructive discussions. The work conducted for this report was funded by the Defence Science and Technology Organisation — Corporate Enabling Research Program (DSTO-CERP).

REFERENCES

1. Callus, P. J., "Novel concepts for conformal load-bearing antenna structure," *Defence Science and Technology Organisation*, DSTO-TR-2096, Australia, February 2008.
2. Golfman, Y., *Hybrid Anisotropic Materials for Structural Aviation Parts*, 199–239, 2010.
3. Niu, M. C. Y., *Composite Airframe Structures*, 2nd edition, Hong Kong Connilit Press Ltd., Hong Kong, 1996.
4. Miles, P. and D. R. Francis, "Carbon fibre reinforced plastic waveguide elements," Great Britain Patent 2, 193, 381, February 3, 1988.
5. Knutsson, L., S. Brunzell, and H. Magnusson, "Mechanical design and evaluation of a slotted CFRP waveguide antenna," *Proceedings of the Fifth International Conference on Composite Materials*, 475–481, San Diego, CA, July 29–August 1, 1985.
6. Wills, K. G., "Improvements relating to electro-deposition," Great Britain patent 1, 283, 916, August 2, 1972.
7. Wagner, R. and H. M. Braun, "A slotted waveguide array antenna from carbon fibre reinforced plastics for the European space SAR," *Acta Astronautica*, Vol. 8, No. 3, 273–282, March 1981.

8. Zienkiewicz, O. C. and R. L. Taylor, *The Finite Element Method*, 5th edition, Elsevier, Oxford, 2000.
9. Czendes, Z. J. and P. Silvester, "Numerical solution of dielectric loaded waveguides: I — Finit-element analysis," *IEEE Transactions on Microwave Theory and Techniques*, Vol. 18, No. 2, 1124–1131, 1970.
10. Daly, P., "Hybrid-mode analysis of microstrip by finite element method," *IEEE Transactions on Microwave Theory and Techniques*, Vol. 19, No. 1, 19–25, 1971.
11. Saad, S. M., "Review of numerical methods for the analysis of arbitrarily-shaped microwave and optical dielectric waveguides," *IEEE Transactions on Microwave Theory and Techniques*, Vol. 33, No. 10, 894–899, 1985.
12. Ansoft HFSS 12.1.2, online resource, 2010.
13. Hexcel Corporation, HexTow IM7 Carbon Fibre Product Data Sheet.
14. Galehdar, A., W. S. T. Rowe, K. Ghorbani, P. J. Callus, S. John, and C. H. Wang, "The effect of ply orientation on the performance of antennas in or on carbon fibre composites," *Progress In Electromagnetics Research*, Vol. 116, 123–136, 2011.
15. Rmili, H., J. L. Miane, H. Zangar, and T. E. Olinga, "Microwave conductivity measurements of high conductive polyaniline films," *Eur. Phys. J. Appl. Phys.*, 65–72, 2005.
16. Nataros, B. M, *Electromagnetics*, Pearson, Boston, 2011.
17. Cytec Engineering Materials, HMF 977-3 Carbon Prepreg data sheet.
18. Nicholson, K. J. and P. J. Callus, "Antenna patterns from single slots in carbon fibre reinforced plastic waveguides," *Defence Science and Technology Organisation*, DSTO-TR-2389, Australia, February 2010.
19. Paul, L., D. R. Corson, and F. Lorrain, *Electromagnetic Fields and Waves*, 3rd edition, W. H. Freeman and Company, New York, 1988.
20. Charles, A. H., *Introduction to Electromagnetic Fields and Waves*, John Wiley & Sons, Inc., New York, 1963.